Progress of Theoretical Physics, Vol. 76, No. 6, December 1986

Production of Hypernuclear States by the (π^+, K^+) Reaction

Hiroharu BANDŌ and Toshio MOTOBA*

Division of Mathematical Physics, Fukui University, Fukui 910
**Laboratory of Physics, Osaka Electro-Communication University Neyagawa 572*

(Received June 9, 1986)

The (π^+, K^+) reaction cross sections are calculated for the ^{12}C, ^{56}Fe and ^{208}Pb targets by using the DDHF single-particle wave functions and employing the meson distorted waves under the eikonal approximation. Characteristics of the (π^+, K^+) reaction are discussed in comparison with the (K^-, π^-) and (stopped K^-, π^-) reactions. A test of the ΛN repulsive pairing is proposed.

§ 1. Introduction

With the epoch-making success of the recoilless (K^-, π^-) reaction experiments done at CERN in the middle of 1970's,[1] hypernuclear physics entered into new stage of development and has revealed various intriguing aspects of strangeness-nuclei.[2] In addition to the recoilless $(K^-, \pi^\pm)$ reactions which exclusively produce the substitutional states, the (stopped $K^-, \pi^\pm$) reactions were introduced at KEK with the aim of populating more varieties of hypernuclear states and have attained a great success especially in the Σ-hypernuclear production.[3] Another challenge is the use of the (π^+, K^+) reaction, the applicability of which was first studied by Dover, Ludeking and Walker.[4] The first trial of the (π^+, K^+) experiment was done at BNL[5] and showed its usefulness if performed extensively.

The (π^+, K^+) reaction gives a sizable amount of momentum transfer, $q > 300$ MeV/c, to the produced hyperon. Since this q is comparable to the nuclear Fermi momentum k_F, it is expected to selectively produce high-spin (J) states, e.g., $[j_n^{-1} j_\Lambda]_{J \simeq j_n + j_\Lambda}$.[4] This feature is welcome particularly for the purposes such as;

1) to see hyperon single-particle states (deeply bound, if possible) in heavy hypernuclei,

2) to know the effective YN particle-hole interaction,

3) to test the predicted repulsive 0^+ pairing in the effective ΛN interaction,[6]

4) to observe "genuinely hypernuclear states"[7] predicted to purely appear in some light hypernuclei, and so forth.

In this paper we restudy the (π^+, K^+) reaction with special reference to the above purposes. We also pay attention to the difference between the (π^+, K^+) and (stopped K^-, π^-) reactions. In § 2, the DWIA treatment with the eikonal approximation for the meson distorted waves is briefly described. In § 3, single-particle energies and wave functions of nucleons and Λ are evaluated with the density-dependent Hartree-Fock (DDHF) method. Section 4 is devoted to the presentation of the calculated results on the production of the Λ-particle neutron-hole states in, as examples, $^{12}_{\Lambda}$C, $^{56}_{\Lambda}$Fe and $^{208}_{\Lambda}$Pb. In § 5, it is argued that an intriguing aspect of ΛN repulsive pairing should be able to be observed by comparing the (K^-, π^-) and (π^+, K^+) excitation spectra.

§ 2. The DWIA treatment

With the spin-flip component neglected as small, the ${}^{A}Z(J_i)(\pi^+, K^+){}^{A}_{\Lambda}Z(J_f)$ reaction cross section is given in DWIA by[8]

$$(\pi^+, K^+): \quad \frac{d\sigma_{if}(\theta)}{d\Omega_L}=\frac{d\mathring{\sigma}(\theta)}{d\Omega_L}N_{\rm eff}^{(\pi K)}(i\to f;\theta)\,, \tag{2·1}$$

where $d\mathring{\sigma}/d\Omega_L$ is the cross section of the elementary $\pi^+ + n\to \Lambda + K^+$ process in the laboratory system. The effective neutron number $N_{\rm eff}$ carries the effects of the nuclear and hypernuclear structures, the momentum matching and the distortion of the meson waves. It is given by

$$N_{\rm eff}^{(\pi K)}(i\to f;\theta)=\frac{1}{[J_i]}\sum_{M_iM_f}|\langle J_fM_f|H_{\pi^+K^+}|J_iM_i\rangle|^2 \tag{2·2}$$

with

$$H_{\pi^+K^+}=\int d^3\boldsymbol{r}\,\chi^{(-)}_{\boldsymbol{p}_K}(\boldsymbol{r})^*\chi^{(+)}_{\boldsymbol{p}_\pi}(\boldsymbol{r})\sum_{j=1}^{A}u_-(j)\delta(\boldsymbol{r}-\boldsymbol{r}_j)\,, \tag{2·3}$$

where the u-spin lowering operator u_- converts a neutron into a Λ-particle. The energy conservation imposes a relation

$$\sqrt{m^2_{\pi^+}+p^2_{\pi^+}}+M_N+E(J_i)=\sqrt{m^2_{K^+}+p^2_{K^+}}+M_\Lambda+E(J_f)\,. \tag{2·4}$$

With the partial wave expansion

$$\chi^{(-)}_{\boldsymbol{p}_K}(\boldsymbol{r})^*\chi^{(+)}_{\boldsymbol{p}_\pi}(\boldsymbol{r})=\sum_{km}\sqrt{4\pi}\sqrt{[k]}\,i^k\tilde{f}_{km}(p_\pi, p_K, \theta; r)\,Y_{km}(\hat{\boldsymbol{r}})\,, \tag{2·5}$$

Eq. (2·2) is reduced to

$$N_{\rm eff}^{(\pi K)}(i\to f;\theta)=\frac{4\pi}{[J_i]}\sum_{km}|\langle J_f\|\sum_j u_-(j)\,\tilde{f}_{km}(p_\pi, p_K, \theta; r_j)\,Y_k(\hat{\boldsymbol{r}}_j)\|J_i\rangle|^2\,. \tag{2·6}$$

If the $|J_i\rangle$ and $|J_f\rangle$ states are described by shell-model configurations, Eq. (2·6) is further reduced. In particular, if $|J_i\rangle$ includes a closed-shell configuration $(n_nl_nj_n)^{2j_n+1}_{j_i=0}$ and $|J_f\rangle$ is of $(n_nl_nj_n)^{2j_n}(n_\Lambda l_\Lambda j_\Lambda)^1$, that is, of a particle-hole configuration $[(n_nl_nj_n)^{-1}(n_\Lambda l_\Lambda j_\Lambda)]_{J_f}$, then $N_{\rm eff}$ is simply expressed as

$$\begin{aligned}&N_{\rm eff}^{(\pi K)}(0^+\to[j_n{}^{-1}j_\Lambda]_J;\theta)\\&\quad=[j_\Lambda][j_n]\left(j_\Lambda\frac{1}{2}j_n-\frac{1}{2}|J0\right)^2|\langle n_\Lambda l_\Lambda j_\Lambda\|\tilde{f}_J\|n_nl_nj_n\rangle|^2\,.\\&\qquad(l_\Lambda+l_n+J=\text{even})\end{aligned} \tag{2·7}$$

If the occupation of the $(n_nl_nj_n)$ orbit is not complete, Eq. (2·7) is accordingly modified.

The (stopped K^-, π^-) analogs of the above equations are obtained by replacing the incoming meson wave function $\chi^{(+)}(\boldsymbol{r})$ by the K^--atomic wave function $R_{n_Kl_K}(r)\,Y_{l_KM_K}(\hat{\boldsymbol{r}})$. By employing the partial wave expansion of the outgoing pion wave

$$\chi^{(-)}_{\boldsymbol{p}_\pi}(\boldsymbol{r})^* = \sum_k \sqrt{4\pi}\sqrt{[k]}(-i)^k \tilde{j}_k(p_\pi; r) Y_{k0}(\widehat{\boldsymbol{p}_\pi \boldsymbol{r}}) , \tag{2·8}$$

integrating over the direction of $\boldsymbol{p}_\pi$ and averaging over M_K, we are led to the expression of the effective neutron number $N_{\rm eff}^{(K^- \text{-abs})}$ for the stopped K^- absorption reactions:

$$N_{\rm eff}^{(K^- \text{-abs})}(0^+ \to [j_n^{-1} j_\Lambda]_J) = [j_\Lambda][j_n]\left(j_\Lambda \frac{1}{2} j_n - \frac{1}{2} | J0\right)^2$$
$$\times \sum_k (J0 l_k 0 | k0)^2 | \langle n_\Lambda l_\Lambda j_\Lambda \| \tilde{j}_k(p_\pi; r) R_{n_K l_K}(r) \| n_n l_n j_n \rangle |^2 . \tag{2·9}$$

In the subsequent sections we present the rate given by

$$R(0^+ \to [j_n^{-1} j_\Lambda]_J) = N_{\rm eff}^{(K^- \text{-abs})}(0^+ \to [j_n^{-1} j_\Lambda]_J) / N_{\rm eff}(\text{tot}) , \tag{2·10}$$

where the total effective neutron number is defined here by

$$N_{\rm eff}(\text{tot}) = \int \rho_n(\boldsymbol{r}) | R_{n_K l_K}(r) |^2 d^3\boldsymbol{r} \tag{2·11}$$

and the neutron density $\rho_n(\boldsymbol{r})$ is normalized as

$$\int \rho_n(\boldsymbol{r}) d^3\boldsymbol{r} = N . \tag{2·12}$$

The meson distorted waves χ are evaluated under the eikonal approximation:

$$\chi^{(+)}_{\pi^+}(\boldsymbol{r}) = \exp\left[i\boldsymbol{p}_\pi \boldsymbol{r} - i v_\pi^{-1} \int_{-\infty}^{z} U_\pi(\sqrt{b^2 + \xi^2}) d\xi \right] , \tag{2·13}$$

$$\chi^{(-)}_{K^+}(\boldsymbol{r})^* = \exp\left[-i\boldsymbol{p}_K \boldsymbol{r} + i v_K^{-1} \int_{z}^{\infty} U_K^*(\sqrt{B^2 + \Xi^2}) d\Xi \right] , \tag{2·14}$$

where

$$\begin{aligned} &\hat{\boldsymbol{p}}_{\pi^+} \cdot \hat{\boldsymbol{p}}_{K^+} = \cos\theta , \\ &\hat{\boldsymbol{p}}_{\pi^+} \cdot \hat{\boldsymbol{r}} = \cos\theta_r , \qquad b = r\sin\theta_r , \qquad z = r\cos\theta_r , \\ &\hat{\boldsymbol{p}}_{K^+} \cdot \hat{\boldsymbol{r}} = \cos\Theta_r , \qquad B = r\sin\Theta_r , \qquad Z = r\cos\Theta_r . \end{aligned} \tag{2·15}$$

The optical potentials U are simply taken as

$$U_m(r) = -i\frac{v_m}{2} \bar{\sigma}_{mN}(1 - i\alpha_m)\rho_N(r) , \qquad m = \pi^+ \text{ or } K^+ , \tag{2·16}$$

where $\bar{\sigma}_{mN}$, α_m and $\rho_N(r)$ indicate the $m+N$ average total cross section, the parameter representing the real potential and the nuclear density distribution, respectively.

The π^- distorted wave associated with the (stopped K^-, π^-) reaction is given analogously to Eq. (2·14). The K^--atomic wave function $R_{n_K l_K}(r)$ is obtained by taking into account the absorption effect, the finite-size effect and so on, with the aid of the computer code made by Seki, Yazaki and Masutani.[9]

§ 3. Single-particle energies and wave functions of Λ and nucleons

The Density-Dependent-Hartree-Fock (DDHF) approach[10),11)] is applied to the calculation of the single-particle (s.p.) energies and wave functions $(\varepsilon_\Lambda, \phi_\Lambda)$, (ε_n, ϕ_n) and (ε_p, ϕ_p). The Skyrme-type effective interactions *SIII*[12)] for *NN* and Rayet # 13[10)] for ΛN are used.

Table I lists the calculated s.p. energies in (^{12}C, $^{12}_{\Lambda}$C), (^{56}Fe, $^{56}_{\Lambda}$Fe) and (^{208}Pb, $^{208}_{\Lambda}$Pb). As

Table I. Single-particle energies ε_n, ε_p and ε_Λ for $^{12}_{\Lambda}$C, $^{56}_{\Lambda}$Fe and $^{208}_{\Lambda}$Pb calculated by employing the DDHF approach with *SIII NN* and Rayet # 13 ΛN interactions. For $^{12}_{\Lambda}$C, the ΛN interaction strength was slightly weakened so as to get $\varepsilon_\Lambda(0p) \approx 0$.

	$^{12}_{\Lambda}$C			$^{56}_{\Lambda}$Fe			$^{208}_{\Lambda}$Pb		
	ε_n	ε_p	ε_Λ	ε_n	ε_p	ε_Λ	ε_n	ε_p	ε_Λ
$0s_{1/2}$	−34.0	−27.7	−10.2	−47.9	−41.8	−19.5	−50.3	−41.2	−22.4
$0p_{3/2}$	−17.6	−11.7	−0.1	−37.5	−31.4	−13.4	−45.6	−36.8	−19.4
$0p_{1/2}$			−0.1	−35.1	−29.2	−13.4	−45.1	−36.3	−19.4
$0d_{5/2}$				−26.3	−20.3	−6.1	−39.8	−31.1	−15.7
$0d_{3/2}$				−21.1	−15.4	−6.1	−38.6	−29.8	−15.7
$1s_{1/2}$				−20.9	−14.9	−3.9	−36.2	−26.8	−14.2
$0f_{7/2}$				−14.9	−9.1	1.6	−33.2	−24.6	−11.4
$0f_{5/2}$						1.6	−30.9	−22.3	−11.4
$1p_{3/2}$	------	------	------	−8.9		0.8	−28.0	−18.7	−8.9
$1p_{1/2}$						0.8	−26.9	−17.7	−8.9
$0g_{9/2}$							−26.0	−17.4	−6.5
$0g_{7/2}$							−22.2	−13.6	−6.5
$1d_{5/2}$							−19.7	−10.4	−3.4
$1d_{3/2}$							−17.7	−8.6	−3.4
$0h_{11/2}$							−18.3	−9.7	−1.2
$2s_{1/2}$	------	------	------	------	------	------	−17.2	−7.5	−2.6
$0h_{9/2}$							−12.7		−1.2
$0i_{13/2}$							−10.2		4.4
$1f_{7/2}$							−11.3		1.5
$1f_{5/2}$							−8.5		1.5
$2p_{3/2}$							−8.2		0.9
$2p_{1/2}$			(all entries are in MeV)				−7.2		0.9

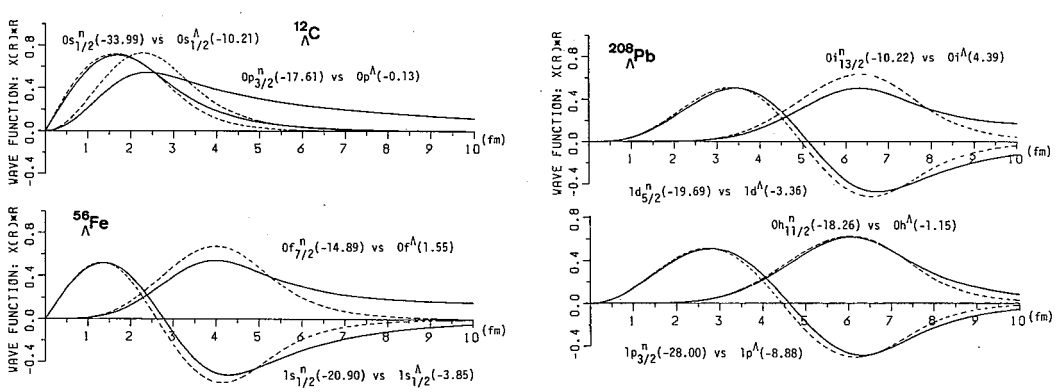

Fig. 1. Illustration of single-particle wave functions for neutrons (dashed) and Λ (solid) with their energies (in MeV) calculated within the density-dependent Hartree-Fock (DDHF) method.

no ΛN ***LS*** interaction is included, Λspin-orbit partners turn out to be degenerate in energy, which is consistent with the empirical fact.[1)]

In Fig. 1 we show some of the s.p. wave functions, ϕ_Λ and ϕ_n, to be compared to each other. For the same orbit, ϕ_Λ is considerably more extended than ϕ_n, reflecting shallower Λ s.p. potential.

The neutron and nuclear densities, $\rho_n(r)$ and $\rho_N(r)$, necessary for Eqs. (2·11) and (2·16) are evaluated from the DDHF wave functions $\phi_N(r)$. The DDHF densities are known to nicely reproduce the observed ones.

§ 4. Results and discussion

—— (π^+, K^+) *vs* (*stopped* K^-, π^-) *vs* (K^-, π^-) ——

We present the calculated results on the production of [n-hole Λ-particle] states in the ${}^{12}_{\Lambda}$C, ${}^{56}_{\Lambda}$Fe and ${}^{208}_{\Lambda}$Pb hypernuclei. Adopted parameters are the following:

(π^+, K^+)

$$p_{\pi^+}=1040\ \mathrm{MeV}/c\,, \qquad \text{(typical transferred momentum } q\sim 330\ \mathrm{MeV}/c\text{)}$$

$$\bar{\sigma}_{\pi^+N}=41\ \mathrm{mb}\,, \qquad \bar{\sigma}_{K^+N}=14\ \mathrm{mb}\,, \qquad \alpha_{\pi^+}=\alpha_{K^+}=0\,. \tag{4·1}$$

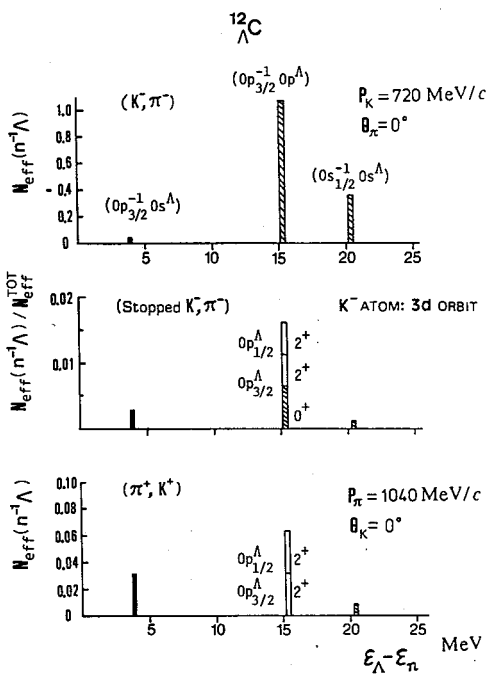

Fig. 2. The calculated excitation spectra of ${}^{12}_{\Lambda}$C due to the (K^-, π^-), (π^+, K^+) and (stopped K^-, π^-) reactions. Each vertical line indicates the strength summed over $j_\Lambda = l_\Lambda \pm \frac{1}{2}$ and J of $[(n_n l_n j_n)^{-1}(n_\Lambda l_\Lambda j_\Lambda)]_J$, which are assumed to be degenerate. The abscissa is given in $\varepsilon_\Lambda(n_\Lambda l_\Lambda) - \varepsilon_n(n_n l_n j_n)$.

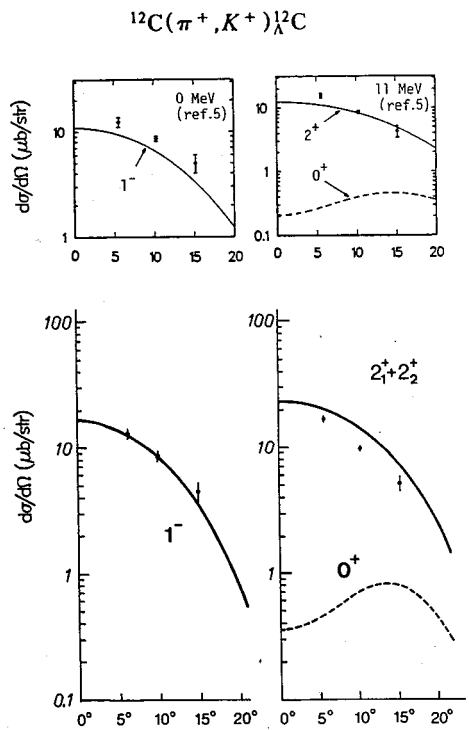

Fig. 3. The calculated angular distributions of K^+ from the ${}^{12}\mathrm{C}(\pi^+, K^+){}^{12}_{\Lambda}\mathrm{C}([n^{-1}\Lambda]_J)$ reaction. Those from Ref. 5) are given for reference.

(stopped K^-, π^-)

(typical $q \sim 280$ MeV/c)

K^--atomic orbit $(n_K l_K)=(3d)$ for ^{12}C;

$(4f)$ for ^{56}Fe,

$(7i)$ for ^{208}Pb,

$\bar{\sigma}_{\pi^- N}=120$ mb, $\quad a_{\pi^-}=0$. (4·2)

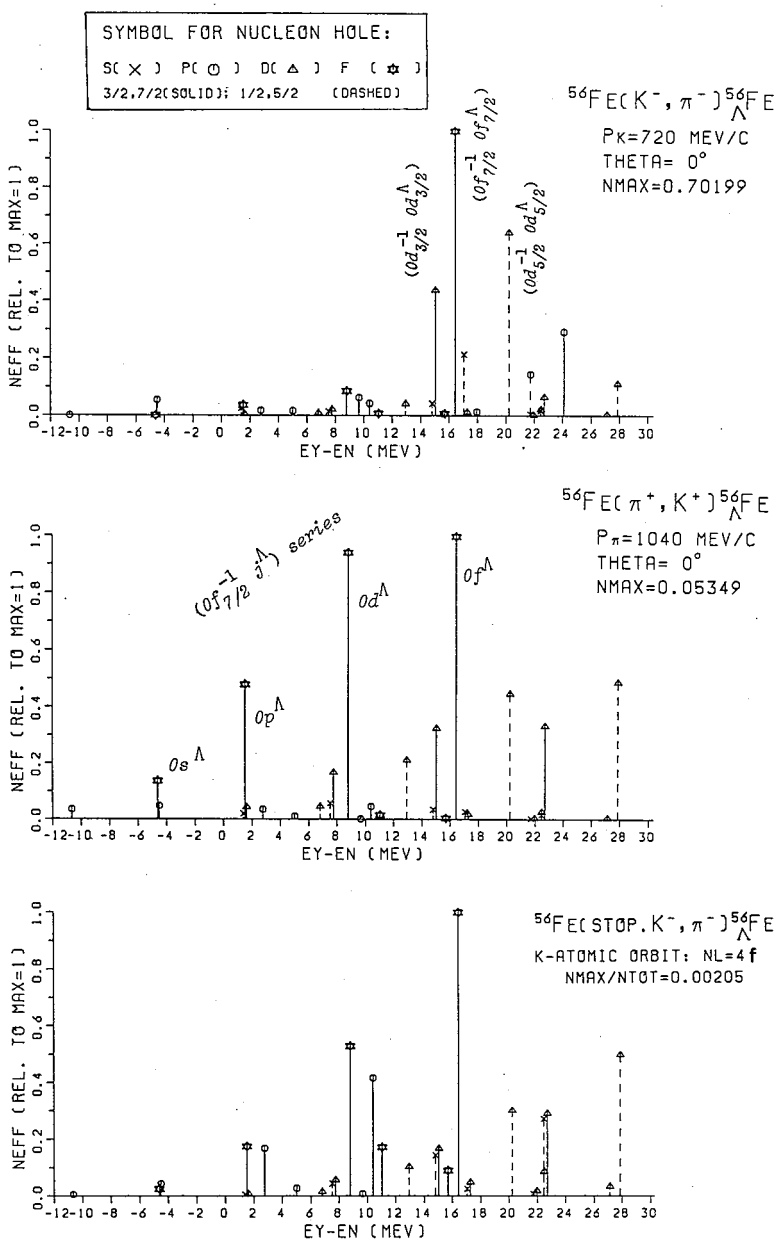

Fig. 4. The calculated excitation spectra of $^{56}_{\Lambda}$Fe due to the (K^-, π^-), (π^+, K^+) and (stopped K^-, π^-) reactions. Comments as for Fig. 2.

(K^-, π^-)

$$p_{K^-}=720\ \mathrm{MeV}/c\,, \qquad (\text{typical } q\sim 50\ \mathrm{MeV}/c)$$

$$\bar{\sigma}_{K^-N}=30\ \mathrm{mb}\,, \qquad \bar{\sigma}_{\pi^-N}=30\ \mathrm{mb}\,, \qquad \alpha_{K^-}=\alpha_{\pi^-}=0\,. \tag{4·3}$$

Although $\bar{\sigma}$ should be somewhat different depending on the momentum of the outgoing meson, which in turn depends on the produced hypernuclear state, we simply take a constant value appropriate for the relevant range of momentum. The parameters α are put zero, as they are not well determined and also not very influential on the results.

Figure 2 shows the calculated excitation spectra of ${}^{12}_{\Lambda}$C due to (K^-, π^-), (π^+, K^+) and (stopped K^-, π^-). The J-multiplet of $(n^{-1}\Lambda)_J$ is put degenerate and the summed value is indicated by the vertical line. The abscissa is given in $(\varepsilon_\Lambda - \varepsilon_n)$, which increases as the excitation energy becomes higher.

A characteristic of the (π^+, K^+) process, large momentum transfer, is seen already in this light hypernucleus as the relatively strong enhancement of the non-substitutional state $(0p^{-1}_{3/2,n}0s_{1/2,\Lambda})$. This feature was actually observed by the experiment.[5] The (π^+, K^+) and (stopped K^-, π^-) reactions start to show their different natures even in this light system, which will become more distinct in heavier hypernuclei.

Figure 3 shows the K^+ angular distributions for the states of ${}^{12}_{\Lambda}$C. Agreement with the experimental data seems quite nice, although our wave functions without any configuration mixing are not so good as those of Ref. 5).

Figures 4 and 5 display the calculated excitation spectrum and angular distributions of ${}^{56}_{\Lambda}$Fe, respectively. Characteristics of the (K^-, π^-), (π^+, K^+) and (stopped K^-, π^-) reactions can be clearly seen in Fig. 4. Figure 6 compares the J-dependences of $N_{\mathrm{eff}}([n^{-1}\Lambda]_J)$ in the (π^+, K^+) and (K^-, π^-) reactions. The contrast is remarkable. The (π^+, K^+) process with large momentum transfer favors high-J states, while low-J states

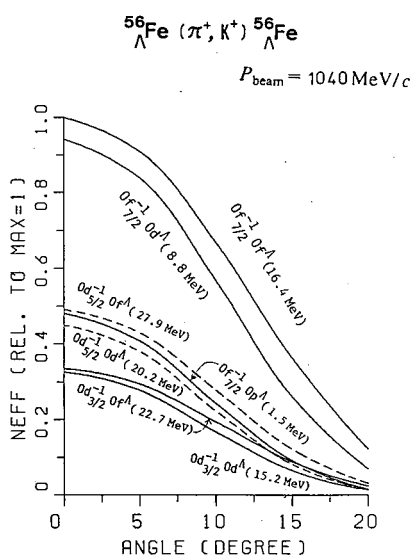

Fig. 5. The calculated angular distributions of K^+ from the ${}^{56}\mathrm{Fe}(\pi^+, K^+){}^{56}_{\Lambda}\mathrm{Fe}([n^{-1}\Lambda]_J)$ reaction. The energies in parentheses correspond to $\varepsilon_\Lambda - \varepsilon_N$ in Fig. 4.

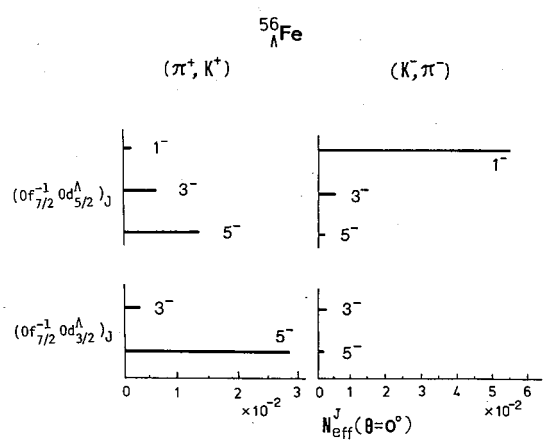

Fig. 6. Comparison of the J-dependences of $N_{\mathrm{eff}}([n^{-1}\Lambda]_J)$ for the (K^-, π^-) and (π^+, K^+) reactions on ^{56}Fe.

are selected by the recoilless-like (K^-, π^-) process.

Let us go up to a heavy hypernucleus $^{208}_{\Lambda}$Pb, in which the advantageous character of the (π^+, K^+) reaction is disclosed in the most evident way. First we show the excitation spectra for the (π^+, K^+) and (stopped K^-, π^-) reactions in Fig. 7, where six neutron-hole orbits, $0i_{13/2}$, $0h_{9/2}$, $1f_{7/2}$, $1f_{5/2}$, $2p_{3/2}$ and $2p_{1/2}$, are included. Selective nature of the reactions is much more significant in (π^+, K^+) than in (stopped K^-, π^-). In (π^+, K^+), the $(n^{-1}\Lambda)$ pairs with nodeless s.p. wave functions acquire particularly strong populations and constitute a beautiful series of peaks, while in (stopped K^-, π^-) strengths are distributed among many states, resulting in a dense spectrum.

Another interesting difference is in the J-dependence of the strengths leading to $(n^{-1}\Lambda)_J$ states, which is evident in the examples shown in Fig. 8. The (π^+, K^+) reaction always favors high-J states, while the (stopped K^-, π^-) reaction enhances low-J states for

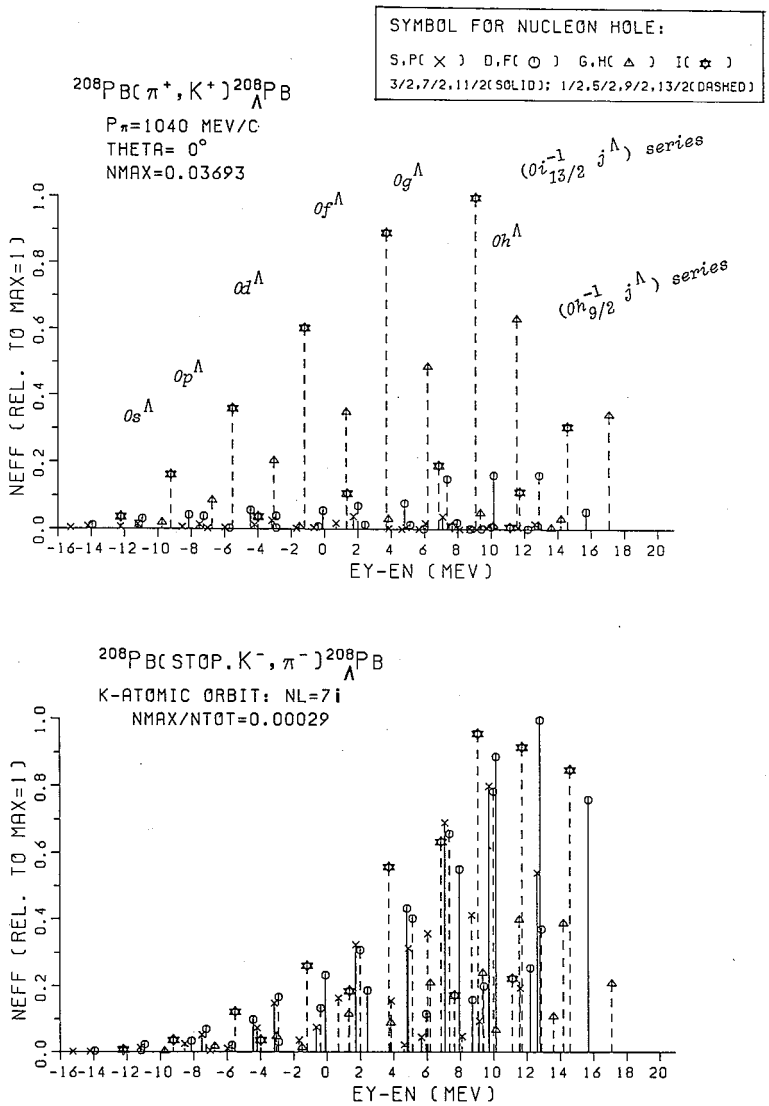

Fig. 7. The calculated excitation spectra of $^{208}_{\Lambda}$Pb due to the (π^+, K^+) and (stopped K^-, π^-) reactions. Comments as for Fig. 2.

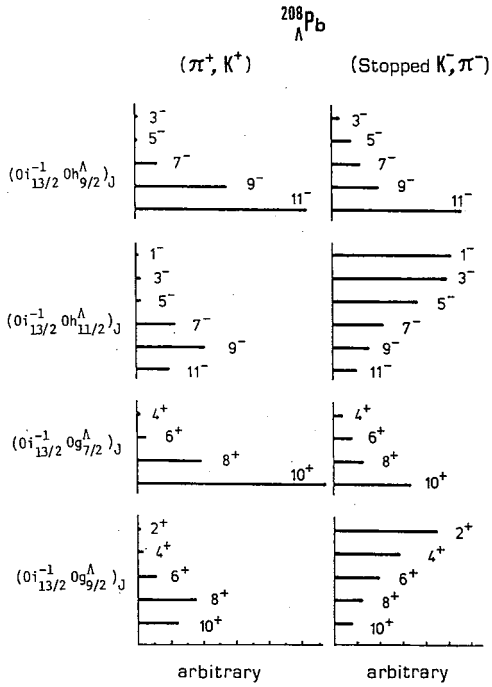

Fig. 8. Comparison of the J-dependences of $N_{\rm eff}([n^{-1}\Lambda]_J)$ for the (π^+, K^+) and (stopped K^-, π^-) reactions on ^{208}Pb.

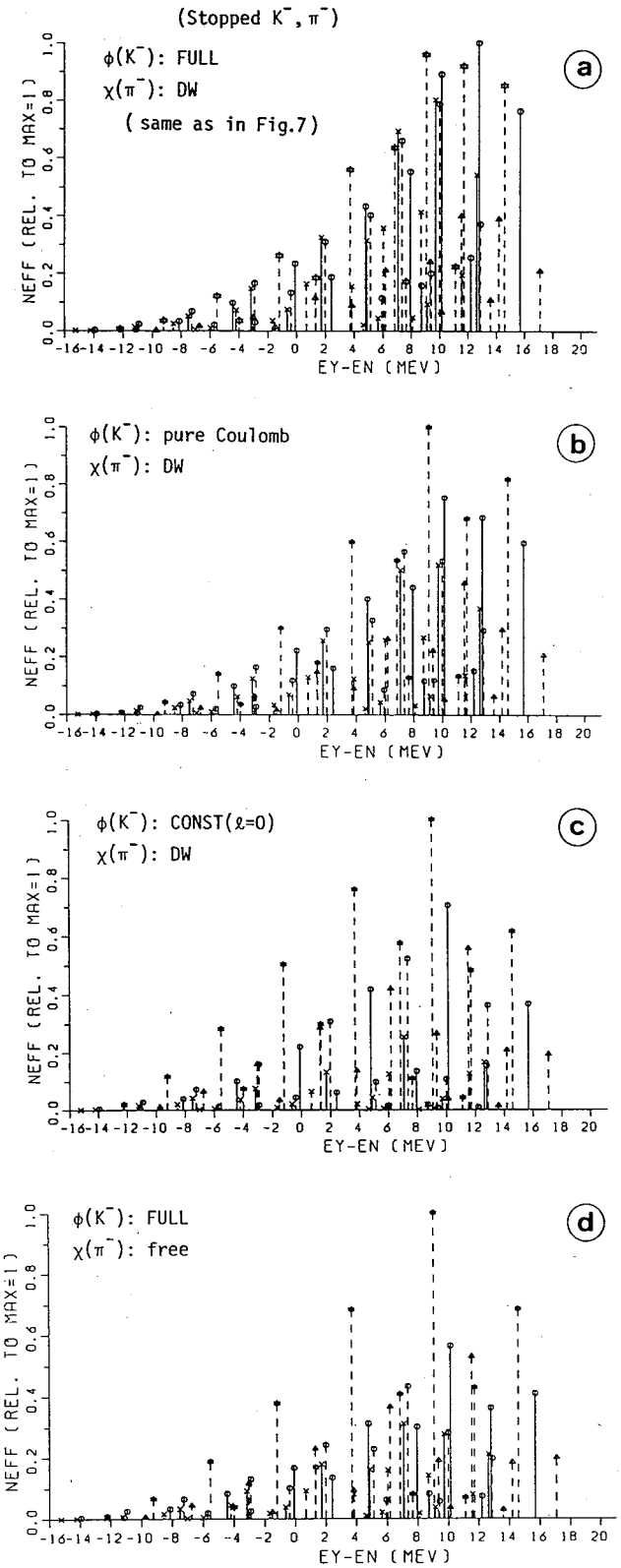

$(j^{-1}_{>,n}j_{>,\Lambda})$ and $(j^{-1}_{<,n}j_{<,\Lambda})$ pairs and high-J states for $(j^{-1}_{>,n}\ j_{<,\Lambda})$ and $(j^{-1}_{<,n}j_{>,\Lambda})$ pairs. The reason can be understood by comparing Eqs. (2·7) and (2·9). The CG-coefficients $(j_\Lambda\ \frac{1}{2}\ j_n - \frac{1}{2}\,|J0)^2$ possess a kinematical property which is exactly the same as that described above for (stopped K^-, π^-). However, the matrix elements $\langle n_\Lambda l_\Lambda j_\Lambda \| \tilde{j}_J \| n_n l_n j_n \rangle$ for (π^+, K^+) are so strongly peaked at high J that this aspect persists in the final result. In (stopped K^-, π^-), the coupling with the angular momentum l_K of the K^--atom diffuses the property of the matrix element over a wide range of J and consequently the result follows the J-dependence of the CG-coefficient.

In order to see what effects underlie the different features of Fig. 7, let us display a series of figures obtained by switching off

(continued)

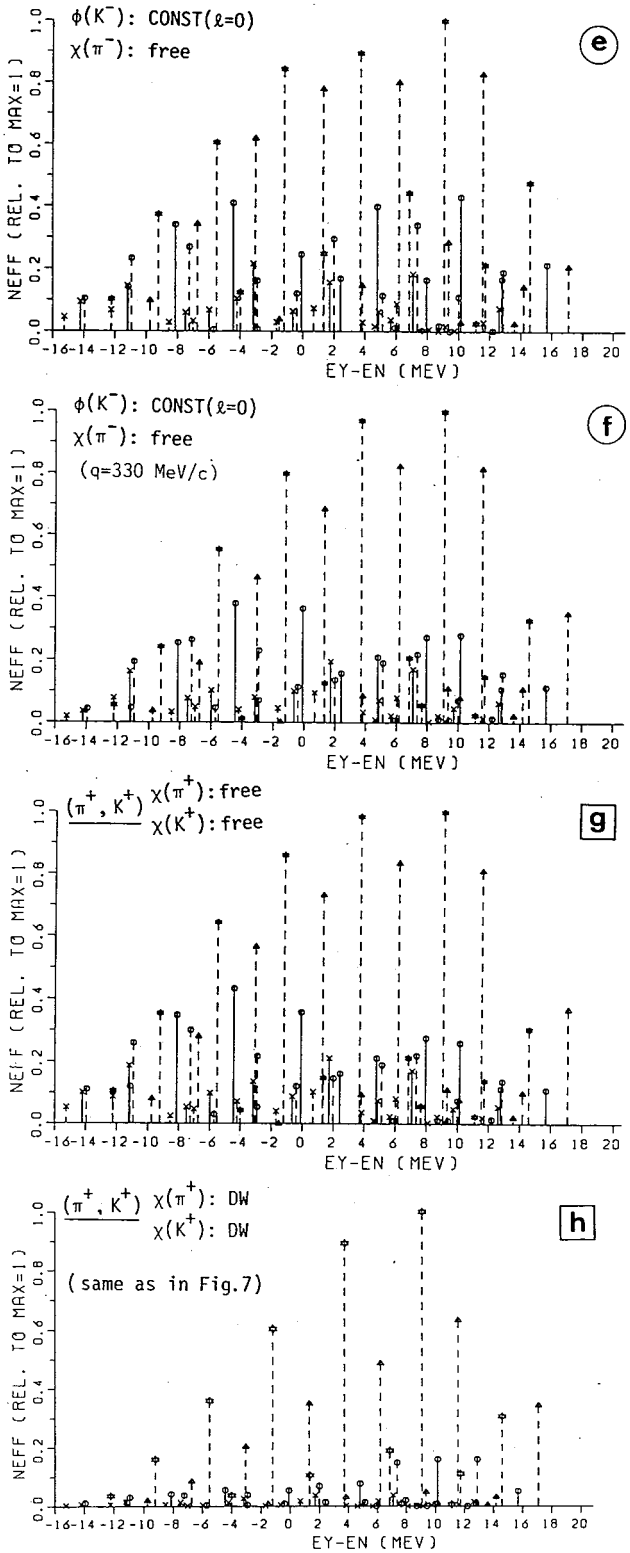

Fig. 9. Variation of the excitation spectrum according to switching off some effects. See the text and the labels on the figures for details.

some effects. In Fig. 9, from top to bottom, (a) ^{208}Pb (stopped K^-, π^-)$^{208}_{\Lambda}$Pb, full effects (same as in Fig. 7), (b) pure Coulomb wave function for the K^--atom, (c) s-state and no r-dependence (constant) for the K^--atomic wave function, (d) no distortion (free) for the pion wave, (e) free pion wave plus s-state and constant K^--atomic wf, (f) momentum transfer q fixed at 330 MeV/c in addition to (e), (g) ^{208}Pb(π^+, K^+) $^{208}_{\Lambda}$Pb with free π^+ and K^+ waves, (h) (π^+, K^+) full effects (same as in Fig. 7).

Looking through (a) to (h), we find that the dense spectrum by (stopped K^-, π^-) is realized by the coherent effects of the angular momentum mixing due to l_K of the K^--atom, the very strong absorption of π^- with momentum at the Δ region and the magnitude of q $\simeq$280 MeV/c (cf. $\sim$330 MeV/c for (π^+, K^+)).

How the high-J dominating character arises in (π^+, K^+) is illustrated in Fig. 10 by drawing the s.p. wave functions and the distorted waves $\tilde{j}_J(r)$ as functions of r. As is evident from the comparison of $\tilde{j}_J(r)$ with the free waves $j_J(qr)$, low-J partial waves undergo serious absorption and therefore even the low-l orbits with inner amplitude cannot get significant strengths. The wave functions of high-l orbits just take maximum overlaps with high-J partial waves $\tilde{j}_J(r)$.

§ 5. Test of the ΛN repulsive pairing

In contrast to the NN interaction, the ΛN $J=0^+$ pairing inter-

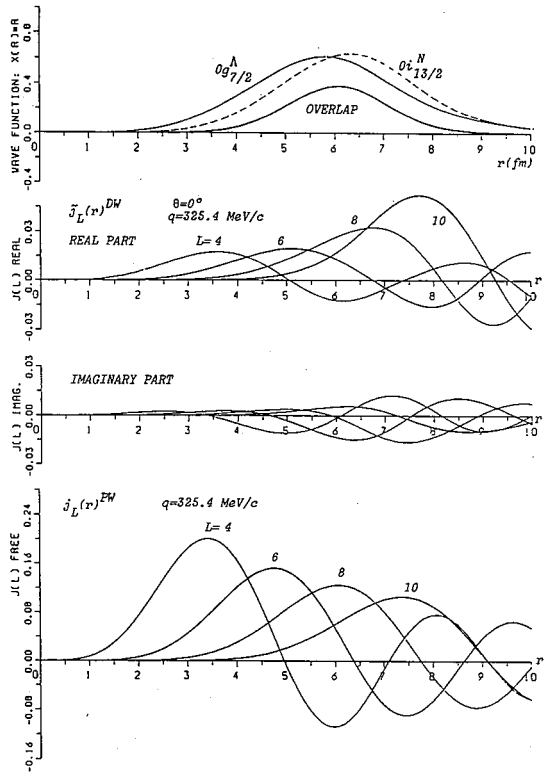

Fig. 10. Illustration of the s.p. wave functions $\phi_n(r)$ and $\phi_\Lambda(r)$ and the (π^+, K^+) distorted waves $\tilde{j}_L(r)$, which appear in the matrix element $\langle\phi_\Lambda|\tilde{j}_L|\phi_n\rangle$. For comparison, $j_L(qr)$ for free waves are also shown.

action is coherently repulsive.[6] The reason is that the balance between the inner repulsive core and the outer attractive potential is much more delicate in ΛN than in NN. In the NN case, however close the two nucleons confined in a j-shell approach each other, they feel a net attraction, giving an attractive $J=0^+$ pairing. In the ΛN case, however, the balance is so delicate that a ΛN pair in the $J=0^+$ state feels more repulsion than attraction.

Figure 11 displays the $\langle 0d^n_{5/2}0d^n_{5/2}|v^{\rm eff}_{NN}|0d^n_{5/2}0d^n_{5/2}\rangle_J$ and $\langle 0d^\Lambda_{5/2}0d^n_{5/2}|v^{\rm eff}_{\Lambda N}|0d^\Lambda_{5/2}0d^n_{5/2}\rangle_J$ matrix elements against J. The HNY potential[13] and the YNG potential[14] are respectively used for $v^{\rm eff}_{NN}$ and $v^{\rm eff}_{\Lambda N}$, which simulate the G-matrices for the $G3RS$[15] and the Nijmegen model D[16] by three-range Gaussian form. The J-dependences of the NN and ΛN matrix elements are more or less parallel except for the pairing $J=0^+$. If this repulsive nature of the ΛN pairing can be tested by experiment, it might be a rare case to be able to prove the existence of the repulsive core without high-energy scattering data available.

Let us consider the $^{18}O(K^-, \pi^-)^{18}_{\Lambda}O$ and $^{18}O(\pi^+, K^+)^{18}_{\Lambda}O$ reactions. Since the target ^{18}O has two valence neutrons in a coherent combination of $(0d_{5/2})^2$, $(1s_{1/2})^2$ and $(0d_{3/2})^2$, the (K^-, π^-) reaction enhances three substitutional-like 0^+ states, of which the coherent one is uppermost in energy and even the lowest 0^+ state is located above the other J states due to the repulsive pairing. On the other hand, the (π^+, K^+) reaction selectively populates the $J=4^+$ state. The situation is shown in Fig. 12.

Thus, by combining the (K^-, π^-) and (π^+, K^+) reactions both with resolution enough to discriminate $\sim$1 MeV, we can test if the repulsive ΛN pairing, namely, the inner repulsive core, really exists.

§ 6. Concluding remarks

In view that the (π^+, K^+) reaction is a promising and just being undertaken method of hypernuclear production, we have studied it with special attention to the comparison with the (K^-, π^-) and (stopped K^-, π^-) reactions. The selective nature of (π^+, K^+) for nodeless $[n^{-1}\Lambda]_J$ with high J becomes very distinct in heavier hypernuclei. The selectivity is much more significant than in (stopped K^-, π^-) in $^{208}_{\Lambda}$Pb for example. It seems to be advantageous to use (π^+, K^+) to see low-lying hyperon orbits in heavy hypernuclei.

In addition, joint use of the (K^-, π^-) and (π^+, K^+) reactions is useful to test the

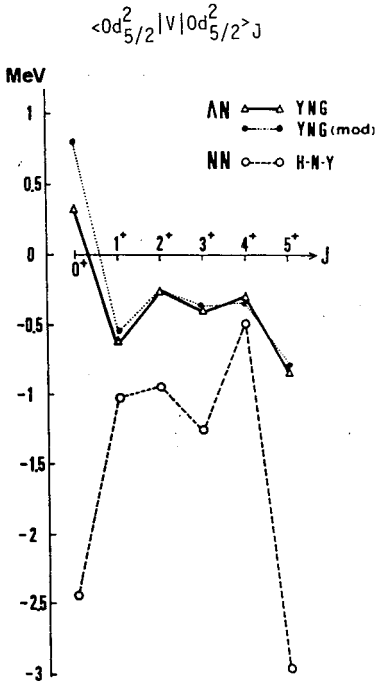

Fig. 11. The $\langle 0d_{5/2}0d_{5/2}|v|0d_{5/2}0d_{5/2}\rangle$ matrix elements of the NN and ΛN interactions drawn against J.

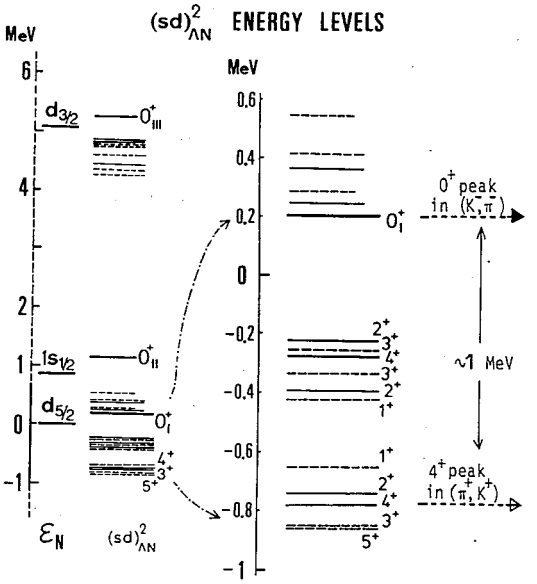

Fig. 12. The ΛN two-particle energy levels calculated within the $(sd)^2$ shell-model space (their expanded version in the right half). The single-particle energies adopted here are empirical for nucleon (ε_N) and degenerate for Λ. These levels consist of a group in the whole spectrum of $^{18}_{\Lambda}$O, where the 0^+ and 4^+ states are expected to be selectively excited by the (K^-, π^-) and (π^+, K^+) processes, respectively.

interesting ΛN repulsive 0^+ pairing predicted on the basis of the existence of the repulsive core.

The basic features of (π^+, K^+) found in this paper should persist in Σ-hypernuclear production. However, in connection with the puzzling narrow Σ widths, we do not really know what are the Σ s.p. states and so at this stage we should refrain from doing some calculations for Σ. For Σ, strong isospin-dependent N-hole Σ-particle interactions have to be taken into account.

Acknowledgements

We would like to thank K. Yazaki, K. Nakai, H. Ejiri, T. Fukuda, T. Shibata and O. Hashimoto for many useful comments and discussion. One of the authors (H. B.) is partially indebted to the support by the "Grant-in-Aid for Scientific Research of Ministry of Education, Science and Culture". Numerical computations were carried out at the Data Processing Center of Kyoto University.

References

1) W. Brückner et al., Phys. Lett. **55B** (1975), 107; **62B** (1976), 481; **79B** (1978), 157.
B. Povh, Rep. Prog. Phys. **39** (1976), 824; in *Ann. Rev. Nucl. Part. Sci.*, ed. J. D. Jackson et al. (Annual Reviews Inc., Palo Alto, 1978), vol. 28, p. 1.
2) *Proc. Int. Conf. on Hypernuclear and Kaon Physics, 1982, Heidelberg,* MPIH-1982-V20, ed. B. Povh.
Proc. Int. Symp. on Hypernuclear and Kaon Physics, 1985, Brookhaven, ed. R. E. Chrien [Nucl. Phys. **A450** (1986)].
3) T. Yamazaki, T. Ishikawa, K. Yazaki and A. Matsuyama, Phys. Lett. **144B** (1984), 177.
T. Yamazaki et al., Phys. Rev. Lett. **54** (1985), 102.
T. Yamazaki et al., Nucl. Phys. **A434** (1985), 363c.
4) C. B. Dover, L. Ludeking and G. Walker, Phys. Rev. **C22** (1980), 2073.
5) C. Milner et al., Phys. Rev. Lett. **54** (1985), 1237.
6) T. Yamada, T. Motoba, K. Ikeda and H. Bandō, Prog. Theor. Phys. Suppl. No. 81 (1985), Chap. IV.
T. Motoba, Nucl. Phys. **A450** (1986), 209c; Czech. J. Phys. **B36** (1986), 435.
7) H. Bandō, K. Ikeda and T. Motoba, Prog. Theor. Phys. **69** (1983), 918.
T. Motoba, H. Bandō and K. Ikeda, Prog. Theor. Phys. **70** (1983), 189.
8) J. Hüfner, S. Y. Lee and H. A. Weidenmüller, Nucl. Phys. **A234** (1974), 429; Phys. Lett. **49B** (1974), 409.
A. Bouyssy, Nucl. Phys. **A290** (1977), 324.
R. H. Dalitz and A. Gal, Ann. of Phys. **116** (1978), 167.
9) R. Seki, K. Yazaki and K. Masutani, Y3/GA01 code in the Program Library of the Computer Center, University of Tokyo.
10) M. Rayet, Nucl. Phys. **A367** (1981), 381.
11) H. Bandō and H. Takaki, Prog. Theor. Phys. **72** (1984), 106.
12) D. Vautherin and D. M. Brink, Phys. Rev. **C5** (1972), 626.
13) A. Hasegawa and S. Nagata, Prog. Theor. Phys. **45** (1971), 1786.
Y. Yamamoto, Prog. Theor. Phys. **52** (1974), 471.
14) Y. Yamamoto and H. Bandō, Prog. Theor. Phys. **73** (1985), 905.
15) R. Tamagaki, Prog. Theor. Phys. **39** (1967), 91.
16) M. M. Nagels, T. A. Rijken and J. J. de Swart, Phys. Rev. **D12** (1975), 744; **D15** (1977), 2547.